scientific reports

Check for updates

OPEN

Critical analysis for nonlinear oscillations by least square HPM

Muhammad Rafiq[1], Muhammad Kamran[1], Hijaz Ahmad[2,3,4,5] & Afis Saliu[6]✉

In this study, a novel adapted homotopy perturbation method (HPM) is used to treat the nonlinear phenomena of free vibration in a system with one degree of freedom. This adaptation involves the integration of HPM with a least-squares optimizer, resulting in a hybrid method called the least square homotopy perturbation method (LSHPM). The LSHPM is tested on various nonlinear problems documented in the existing literature. To evaluate the effectiveness of the proposed approach, the identified problems are also tackled using HPM and the MATLAB built-in function bvp5c, and then the results are compared with those obtained using LSHPM. In addition, a comparative analysis is carried out with the results of the AG method as found in the literature. The results show that LSHPM is a reliable and efficient method suitable for solving more complicated initial value problems in the fields of science and engineering.

An oscillation system denotes a dynamic system that demonstrates periodic motion around an equilibrium point. Oscillations are ubiquitous in the natural world, appearing in various physical, mechanical, electrical, and biological systems. A comprehensive understanding of oscillation principles holds paramount importance in disciplines such as physics, engineering, and biology.

Dynamic systems that manifest oscillations or vibrations departing from linearity are referred to as nonlinear oscillating systems.These systems are commonly characterized by nonlinear differential equations, capturing intricate and at times unpredictable dynamics. These kinds of nonlinear oscillatory systems are found in many different scientific and engineering fields, including mechanics[1], electromagnetic phenomena[2], fluid dynamics[3], biology[4–7], chemistry[8], and other fields[9], including particle physics and cosmology[10]. These systems describe several applications of nonlinear oscillating dynamics. A few examples of this diversity are as follows: an electronic circuit that integrates nonlinear components such as diodes or transistors[11]; a pendulum that exhibits significant amplitude swings and displays nonlinear characteristics[12]; a chemical reaction that displays oscillatory tendencies due to nonlinear kinetics[13]; and animal populations that oscillate due to nonlinear interactions[14].

One of the main features of nonlinear oscillatory systems is their sensitivity to initial conditions and parameters. Minor adjustments to these parameters may cause the system to function significantly in a different way, which may lead to the rise of disordered dynamics or other oscillatory types[15]. Despite their intricacy, nonlinear oscillatory systems are an vital area of investigation that suggest critical perceptions into a class of real and synthetic systems. Through in-depth research and modelling, scientists and engineers can learn a deep knowledge of the main procedures of these systems, which they can then use to develop the functionality and shape of various systems. Nonlinear oscillators are currently being intensively explored in a wide range of study disciplines, including as multi-body systems, vibrations, transportation, structural dynamics, and others[16–18].

Various methods, such as He's Energy Balance method[19,20], the Max-Min methodology[2], and the homotopy analysis method[21], have been introduced by researchers to tackle the challenges presented by nonlinear differential equations in oscillatory systems. These methodologies provide effective approaches for analyzing and predicting the behavior of intricate systems.

In 2012, Ganji and Azimi[22] addressed specific nonlinear oscillation systems by applying the max-min technique and developing an amplitude-frequency formulation. In 2022, Samadi et al.[16] tackled similar problems utilizing the AGM and HPM procedures, and they compared their results with those obtained through the RK4 technique. Qie et al.[23] introduced a straightforward and distinctive method for addressing highly nonlinear oscillators. Their study offers an efficient approach to rapidly establish the amplitude-frequency correlation of

[1]Department of Mathematics, COMSATS University Islamabad, Wah Campus, Islamabad, Pakistan. [2]Department of Mathematics, Faculty of Science, Islamic University of Madinah, Madinah, Saudi Arabia. [3]Near East University, Operational Research Center in Healthcare, TRNC Mersin 10, Nicosia, 99138, Turkey. [4]Center for Applied Mathematics and Bioinformatics, Gulf University for Science and Technology, Mishref,, Kuwait. [5]Department of Computer Science and Mathematics, Lebanese American University, Beirut, Lebanon. [6]Department of Mathematics, University of the Gambia, MDI Road, P.O. Box 3530, Kanifing, Serrekunda, The Gambia. ✉email: asaliu@utg.edu.gm

a nonlinear oscillator. The investigation conducted by Mohammadian and colleagues[24] focused on examining the applicability of the AGM and its enhancement for nonlinear damped oscillators. In 2021, El-Dib[25] utilized the HPM technique in conjunction with a rank-upgrading approach to achieve superior results in nonlinear oscillation.

Oscillation systems, commonly encountered in various scientific and engineering disciplines, are frequently characterized and examined using mathematical models. These models serve as reliable instruments for predicting, understanding, and controlling the dynamic features of oscillatory processes. Researchers and engineers can find notable understandings into the complexities of oscillation systems by explaining physical principles into mathematical formulas.

Oscillation systems, distinguished by their rhythmic and repetitive motion, have a close connection with the language of differential equations. This association between oscillations and differential equations offers a robust framework for articulating and comprehending the dynamic characteristics of these systems across various scientific disciplines.

Differential equations serve as a modeling tool for problems involving diverse independent variables[26–28]. This area of study holds significance in mathematics, addressing intriguing issues related to the modeling of various phenomena in physics, biology[29–31], and engineering[32,33]. For instance, phenomena like unsteady squeezing flow of heat and mass transfer[34] and MHD Boundary Layer Flow over a Stretching Sheet[26] find representation through differential equations, as the rate of change is a fundamental expression for describing physical phenomena in scientific investigations[35]. Diverse analytical and numerical methodologies are employed to gain valuable insights into system behavior, unraveling complexities inherent in the study. These approaches encompass the homotopy analysis method[36–38], optimal homotopy asymptotic method[39–41], Adomian decomposition method[42], extended optimal homotopy asymptotic method[39], the coupling of Runge-Kutta methods with the MATLAB neural network built-in function nftool[40,43], the conjunction of the homotopy analysis method with the neural network MATLAB function nftool[40,44], utilization of artificial neural networks[45], the coupling of the MATLAB built-in function nftool with the homotopy asymptotic method[46], and the combination of the Levenberg-Marquardt technique with the MATLAB neural network nftool[35,47].

The HPM has been extensively examined since 1999, evolving into a valuable mathematical tool due to the collaborative efforts of numerous scientists. Researchers have validated the convergence of the ground breaking HPM across various scenarios[48], and diverse modifications have surfaced in the scholarly literature. Upon using the phrase "modified homotopy perturbation method" as a search query in Clarivate Analytics' Web of Science, we identified over 400 relevant items. The combination of HPM with other methods has garnered significant attention, such as the Generalized Differential Quadrature Method[49] and the Fourier transform[50]. The LSHPM, a hybrid of the HPM and the least square method[51,52]. It is Remarkably effective for solving ordinary, partial, and fractional differential equations

In 2012 GANJI1 and AZIMI[22] applied the Max-Min Approach(MMA) and Amplitude Frequency Formulation (AFF) to derive the approximate analytical solution for motion of nonlinear free vibration of conservative, single degree of freedom systems. The results were compared with the results obtained by forth-order runge-kutta method. In 2022 Sanadi et al.[16] used the Akbari Ganji Method, abbreviated as AGM, and the HPM, to analytically investigate some oscillating systems with nonlinear behavior in a variety of situations and compare the results to the numerical approach to assess the validity and accuracy of these methods. The findings in all situations showed the precision of both the AGM and HPM, with all computations showing an amazing similarity to the RK4 method. In this manuscript, we use the newly developed LSHPM and MATLAB builtin functiobn bvp5c to unfold the problem[22]. This method combines HPM with a least squares minimization step, which minimizes approximation errors and speeds up convergence, therefore increasing the method's effectiveness. Compared to other iterative techniques, it provides accurate solutions with fewer iterations. LSHPM is a priceless instrument in a variety of scientific and technical fields due to its many advantages, which include simplicity in using, accuracy, and computational efficacy.

Methodology

We use the newly developed LSHPM and the bvp5c function integrated in MATLAB to solve the problem.

LSHPM

To understand the main idea about the LSHPM, let's examine the following nonlinear differential equation

$$A(v) - g(\xi) = 0, \ \ \xi \in \Omega, \tag{1}$$

with the boundary conditions

$$B(v, \frac{\partial v}{\partial n}) = 0, \ \ \xi \in \Gamma, \tag{2}$$

Equation (1) can be expressed in the following format: A denotes a differential operator of general type, B represents a boundary operator, g is a well-defined analytic function and Γ denotes the boundary surrounding the domain Ω. We have further divided A into its linear and nonlinear summands, L and N, respectively. Consequently, we can reformulate the Eq. (1) as follows

$$L(v) + N(v) - g(\xi) = 0, \ \ \xi \in \Omega. \tag{3}$$

In the Eq. (3), our objective is to solve it using the HPM. To achieve this, we establish a homotopy function $H : \mathbb{R}^n \times [0,1] \longrightarrow \mathbb{R}^m$, for Eq. (3), and this homotopic function H satisfies the convex homotopic property as given below

$$H(v,p) = (1-p)[L(v) - L(v_0)] + p\big[L(v) + N(v) - g(\xi)\big] = 0, \quad \xi \in \Omega, \quad p \in [0,1]. \tag{4}$$

Here, p represents an embedding parameter, while v_0 is an initial approximation of Eq. (1), satisfying the boundary conditions (2). Notably, from Eq. (4), it is evident that

$$H(v,0) = L(v) - L(v_0) = 0, \tag{5}$$

and

$$H(v,1) = L(v) + N(v) - f(\xi) = A(v) - g(\xi) = 0, \quad \xi \in \Omega. \tag{6}$$

The progression of the parameter p from 0 to 1 corresponds to the transformation of $H(v,p)$ from v_0 to v. The function H, parametrized by p, establishes a continuous trajectory from the known initial solution v_0 to the desired solution v. This function is identified as a homotopy linking the functions $H(v,0) = L(v) - L(v_0)$ and $H(v,1) = A(v) - g(\xi)$. Moreover, $L(v) - L(v_0)$ and $A(v) - g(\xi)$ are recognized as homotopic. The symbol $\mathbb{R}$ denotes the set of real values. As the parameter p varies within the interval [0, 1], v_0 progressively converges toward the solution v. It is reasonable to posit that the solution to this equation can be represented as a series involving powers of p, as discussed in references[53].

$$v = v_0 + pv_1 + p^2 v_2 + p^3 v_3 + \cdots. \tag{7}$$

Taking $p \to 1$, estimated result that HPM will produce is

$$\tilde{u} = \lim_{p \to 1} v = v_0 + v_1 + v_2 + v_3 + \cdots. \tag{8}$$

After introducing the unknown constants $c's$ into the derived series solution $\tilde{u}$ given by Eq. (8) as coefficients of $v's$ in order to control the convergence, we designate this new series as $\tilde{U} = \sum_{i=0}^{\infty} c_i v_i$. Subsequently, we substitute the approximate solution $\tilde{U}$ in place of the unknown function v in Eq. (3) to construct the residual function.

$$\hat{R}(\xi, c_i) = L(\tilde{U}) + N(\tilde{U}) - g(\xi), \ \ \xi \in \Omega.. \tag{9}$$

We now determine the residual sum of squares

$$J(c_i) = \int_{\Omega} \hat{R}^2(\xi, c_i) d\xi, \ \ i = 0, \ 1, \ 2, \ \cdots. \tag{10}$$

The optimal values for the unknown constants c_i are established by solving the system of equations $\frac{\partial J}{\partial c_i} = 0$. Afterward, by substituting these determined values of c_i back into $\tilde{U}$, we achieve the desired solution through the application of the Least Square Homotopy Perturbation Method (LSHPM) approach.

bvp5c

The bvp5c code utilizes a finite difference implementation based on the four-stage Lobatto IIIa formula, as described in[54]. This formula, employing collocation, produces a C^1 continuous solution with fifth-order accuracy consistently over the interval $[a, b]$, where $a, b \in \Re$. The implementation adopts the Lobatto IIIa formula as an implicit Runge-Kutta formula. The MATLAB built-in function bvp5c is specifically crafted to directly solve the associated algebraic equations, ensuring a smooth and efficient solution process.

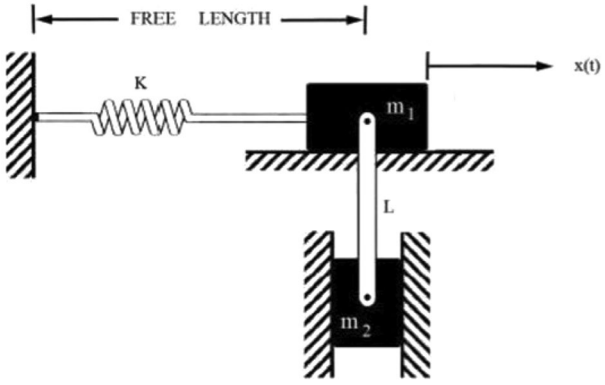

Figure 1. Geometric representation of Case 1.

Oscillating systems

Case 1. In Fig. 1, we assign m_1 as the mass of the horizontal block, and m_2 represents the mass of the vertically displaced block connected to m_1. The symbol L denotes the length, g stands for the acceleration due to gravity, and k represents the spring constant, as illustrated in Fig. 1. Introducing an additional parameter, denoted as v, defined as $v = \frac{x}{L}$, with the condition that $|v| << 1$. With this definition, the differential equation can be expressed in the following manner, as detailed in references[16,22]:

$$\ddot{v} + \ddot{v}v^2\frac{m_2}{m_1} + \frac{m_2}{m_1}v\dot{v}^2 + \left(\frac{k}{m_1} + \frac{gm_2}{Lm_1}\right)v + \frac{gm_2}{2Lm_1}v^3 = 0 \tag{11}$$

In this context, v, $\dot{v}$, and $\ddot{v}$ represent the dimensionless displacement, velocity, and acceleration, respectively, of the vibrating system. The initial displacement and velocity are specified as follows:

$$v(0) = A, \dot{v}(0) = 0. \tag{12}$$

In the presented model, it is apparent that the restoring force of the springs follows a linear pattern. However, the introduction of damping introduces nonlinearity, leading to a mathematical model that deviates from linearity.

Case 2. Figure 2 depicts a simple pendulum with a rod connected to a rotating rigid frame. The rigid frame experiences continuous rotation at an angular velocity represented by Ω around the vertical axis, giving rise to the formulation of the ensuing nonlinear differential equation.[16,22],

$$\frac{d^2\theta}{dt^2} + (1 - \Lambda\cos\theta)\sin\theta = 0, \tag{13}$$

$$\theta(0) = A, \quad \frac{d\theta}{dt}|_{t=0} = 0, \tag{14}$$

where, $\Lambda = \frac{r\Omega^2}{g}$, the variables θ and t are dimensionless and represent displacement and time, respectively. In the context of the Eq. (13), the expression $-\Lambda\cos\theta\sin\theta$ is a result of the movement of the rotating rigid frame.

Consider

$$\sin\theta = \theta - \frac{\theta^3}{3!} + \frac{\theta^5}{5!} - \cdots, \tag{15}$$

and

$$\cos\theta = 1 - \frac{\theta^2}{2!} + \frac{\theta^4}{4!} + \cdots. \tag{16}$$

Substituting (15) and (16) into (13), we have

$$\frac{d^2\theta}{dt^2} - (-1 + \Lambda)\theta + \frac{1}{6}(-2 + 2\Lambda)\theta^3 + \frac{1}{120}(1 - 16\Lambda)\theta^5 = 0. \tag{17}$$

Given that both problems (11) and (17) can be viewed as highly nonlinear in nature. We will apply the HPM, LSHPM and the MATLAB built in function bvp5c to solve these problems.

Implementation of LSHPM

Now, we proceed to address problems (11) and (17) with the help of examples by varying the parameter values.

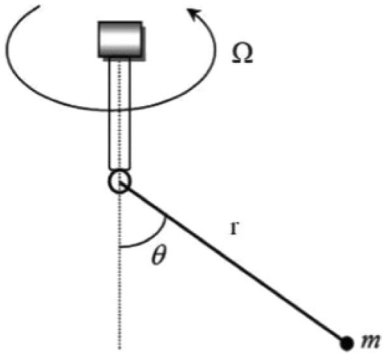

Figure 2. Geometric representation of Case 2.

Example 4.1 By taking $K = 100\,Newton/meter^2$, $g = 9.8meter/sec^2$, $m_1 = 5Kg$ $m_2 = 1Kg$, $L = 1meter$, $A = \frac{\pi}{6} meter$, we rewrite the problem (11) as (11) as

$$\frac{\mathrm{d}^2}{\mathrm{d}t^2}v + \frac{1}{5}v^2\frac{\mathrm{d}^2}{\mathrm{d}t^2}v + \frac{1}{5}v\left(\frac{\mathrm{d}}{\mathrm{d}t}v\right)^2 + \frac{549}{25}\,v + \frac{49}{50}v^3 = 0, \tag{18}$$

$$v(0) = \frac{\pi}{6}, \quad \frac{dv}{dt}|_{t=0} = 0. \tag{19}$$

As previously noted, the initial step in addressing equation (18) using the HPM method involves introducing a constant p as the perturbation factor, which is then integrated into Eq. (18). This results in the formulation of the resultant homotopy equation:

$$H(v,p) = \left\{ (1-p)\left(\tfrac{\mathrm{d}^2}{\mathrm{d}t^2}v + \tfrac{549}{25}\,v\right) + p\left(\tfrac{\mathrm{d}^2}{\mathrm{d}t^2}v + \tfrac{1}{5}v^2\tfrac{\mathrm{d}^2}{\mathrm{d}t^2}v + \tfrac{1}{5}v\left(\tfrac{\mathrm{d}}{\mathrm{d}t}v\right)^2 + \tfrac{549}{25}\,v + \tfrac{49}{50}v^3\right) = 0. \tag{20}$$

Upon substituting Eq. (7) into Eq. (20) and conducting simplifications and rearrangements that are contingent on the powers of p, we can derive the corresponding parameters

$$p^0 : \left\{ \tfrac{\mathrm{d}^2}{\mathrm{d}t^2}v_0 + \tfrac{549}{25}\,v_0 = 0, \right. \tag{21}$$

$$p^1 : \left\{ \tfrac{\mathrm{d}^2}{\mathrm{d}t^2}v_1 + \tfrac{549}{25}\,v_1 + \tfrac{1}{5}\left(\tfrac{\mathrm{d}^2}{\mathrm{d}t^2}v_0\right)v_0^2 + \tfrac{1}{5}\,v_0\left(\tfrac{\mathrm{d}}{\mathrm{d}t}v_0\right)^2 + \tfrac{49}{50}\,v_0^3 = 0, \right. \tag{22}$$

$$p^2 : \left\{ \begin{array}{l} \tfrac{\mathrm{d}^2}{\mathrm{d}t^2}v_2 + \tfrac{549}{25}\,v_2 + \tfrac{2}{5}\left(\tfrac{\mathrm{d}^2}{\mathrm{d}t^2}v_0\right)v_0v_1 + \tfrac{1}{5}\left(\tfrac{\mathrm{d}^2}{\mathrm{d}t^2}v_1\right)v_0^2 + \tfrac{2}{5}\,v_0\left(\tfrac{\mathrm{d}}{\mathrm{d}t}v_0\right)\tfrac{\mathrm{d}}{\mathrm{d}t}v_1 + \tfrac{1}{5}\,v_1\left(\tfrac{\mathrm{d}}{\mathrm{d}t}v_0\right)^2 + \\ \tfrac{147}{50}\,v_0^2v_1 = 0, \end{array} \right. \tag{23}$$

$\vdots$

By solving Eqs. (21)–(23) with appropriate initial conditions, we can ascertain the parameters associated with v_i for $i = 0, 1, 2, \ldots$. It is noteworthy that, except for Eq. (21), the remaining equations are addressed with a zero initial condition. Upon resolving Eqs. (21) through (23), we can determine the values for v_0, v_1, and v_2. Through the synthesis of the solutions to Eqs. (21) through (23), we obtain the approximate solution for Eq. (18) using the HPM in the following manner.

$$v = v_0 + v_1 + v_2.$$

This implies

$$\begin{array}{l} v = 0.0002524761914\,\cos^5(\alpha t) - 0.006546499663\,\cos^3(\alpha t) + 0.5298927993\,\cos(\alpha\, t) - \\ \quad 0.0008175481825\,t\cos^2(\alpha t)\sin(\alpha t) + 0.02200129925\,t\sin(\alpha\, t) - 0.0004781577738\,t^2\cos(\alpha t). \end{array} \tag{24}$$

It is crucial to note that incorporating a greater number of components, such as v_3, v_4, and so forth, within v in Eq. (24) has the potential to further enhance accuracy and minimize errors to a greater extent. Subsequently, Eq. (24) comprises various terms, including $\cos^5(\alpha t)$, $\cos^3(\alpha t)$, $\cos(\alpha t)$, $t\cos^2(\alpha t)\sin(\alpha t)$, $t\sin(\alpha t)$, and $t^2\cos(\alpha t)$, where $\alpha = 4.686149806$. With this information, we propose that our trial solution for Eq. (18) within the LSHPM framework takes the following form:

$$\tilde{v} = c_0\,\cos^5(\alpha t) + c_1\,\cos^3(\alpha t) + c_2\,\cos(\alpha\, t) + c_3\,t\cos^2(\alpha t)\sin(\alpha t) + c_4\,t\sin(\alpha\, t) + c_5\,t^2\cos(\alpha\, t). \tag{25}$$

When we apply the boundary conditions (19) to Eq. (25), we obtain

$$c_0 = \pi/6 - c_1 - c_2. \tag{26}$$

By putting (26) in (25), we have

$$\tilde{v} = \left(\frac{\pi}{6} - c_1 - c_2\right)\cos^5(\alpha t) + c_1\cos^3(\alpha t) + c_2\cos(\alpha\, t) + c_3\cos^2(\alpha t)\sin(\alpha\, t)t + c_4t\sin(\alpha\, t) + c_5t^2\cos(\alpha\, t). \tag{27}$$

We establish the residual function by substituting $\tilde{v}$ in place of v in Eq. (18), we have

$$\hat{R}(t, c_1, c_2, c_3, c_4, c_5) = \frac{\mathrm{d}^2}{\mathrm{d}t^2}\tilde{v} + \frac{1}{5}\left(\frac{\mathrm{d}^2}{\mathrm{d}t^2}\tilde{v}\right)(\tilde{v})^2 + \frac{1}{5}\tilde{v}\left(\frac{\mathrm{d}}{\mathrm{d}t}\tilde{v}(t)\right)^2 + \frac{549}{25}\,\tilde{v} + \frac{49}{50}\,(\tilde{v})^3. \tag{28}$$

Upon performing the computation represented by Eq. (29):

$$J(c_1, c_2, c_3, c_4, c_5) = \int_0^3 \hat{R}^2(t, c_1, c_2, c_3, c_4, c_5), dt, \tag{29}$$

The optimal values for the variables c_i, with i ranging from 1 to 5, can be obtained by calculating the partial derivatives $\frac{\partial J}{\partial c_i}$ using MAPLE 2016 software. Once these optimal values are determined, they can be substituted into the proposed solution as outlined in Eq. (25):

$$\begin{aligned}\tilde{v} = {} & 0.0002205067\,(\cos(4.686149806t))^5 - 0.006357987814\,(\cos(4.686149806t))^3 + \\ & 0.5297362569\,\cos(4.686149806t) - 0.0007420527380\,(\cos(4.686149806t))^2 \sin(4.686149806t)t + \\ & 0.02190612201\,\sin(4.686149806t)t - 0.0004639409468\,\cos(4.686149806t)t^2.\end{aligned} \tag{30}$$

Discussion of results of Example 4.1

The numerical results for both the HPM (22) and the LSHPM (28) are summarized in Table 1, and graphical representations of the HPM solution (22) and the LSHPM solution (28) are presented in Fig. 3.

t	bvp5c	AGM[16]	HPM	LSHPM	$\lvert AGM - bvp5c\rvert$	$\lvert HPM - bvp5c\rvert$	$\lvert LSHPM - bvp5c\rvert$
0	0.52359877	0.52359878	0.5235988	0.52359877	0	0	0
0.3	0.09348159	0.10071564	0.0934789	0.09342673	7.23×10^{-3}	2.62×10^{-6}	5.48×10^{-5}
0.6	− 0.49167124	− 0.48485292	− 0.4916685	− 0.49166608	6.82×10^{-3}	2.69×10^{-6}	5.15×10^{-6}
0.9	− 0.26805498	− 0.28724119	− 0.2680486	− 0.26793718	1.91×10^{-2}	6.40×10^{-6}	1.17×10^{-4}
1.2	0.39917946	0.37434968	0.3991713	0.39918235	2.48×10^{-2}	8.21×10^{-6}	2.88×10^{-6}
1.5	0.40780643	0.43125554	0.4077659	0.40768673	2.34×10^{-2}	4.06×10^{-5}	1.19×10^{-4}
1.8	− 0.25623998	− 0.20844333	− 0.2562237	− 0.25630187	4.78×10^{-2}	1.62×10^{-5}	6.18×10^{-5}
2.1	− 0.49613197	− 0.51144482	− 0.4959898	− 0.49600062	1.53×10^{-2}	1.42×10^{-4}	1.31×10^{-4}
2.4	0.07994805	0.01168773	0.0798925	0.08008753	6.83×10^{-2}	5.55×10^{-5}	1.39×10^{-4}
2.7	0.52342702	0.51594116	0.5231526	0.52325033	7.49×10^{-3}	2.74×10^{-4}	1.76×10^{-4}
3.0	0.10694792	0.18679763	0.1071116	0.10682589	7.98×10^{-2}	1.63×10^{-4}	1.22×10^{-4}

Table 1. Comparison of HPM, LSHPM, AGM and bvp5c results when $k = 100$, $g = 9.8, m_1 = 5, m_2 = 1$, $L = 1, A = \frac{\pi}{6}$.

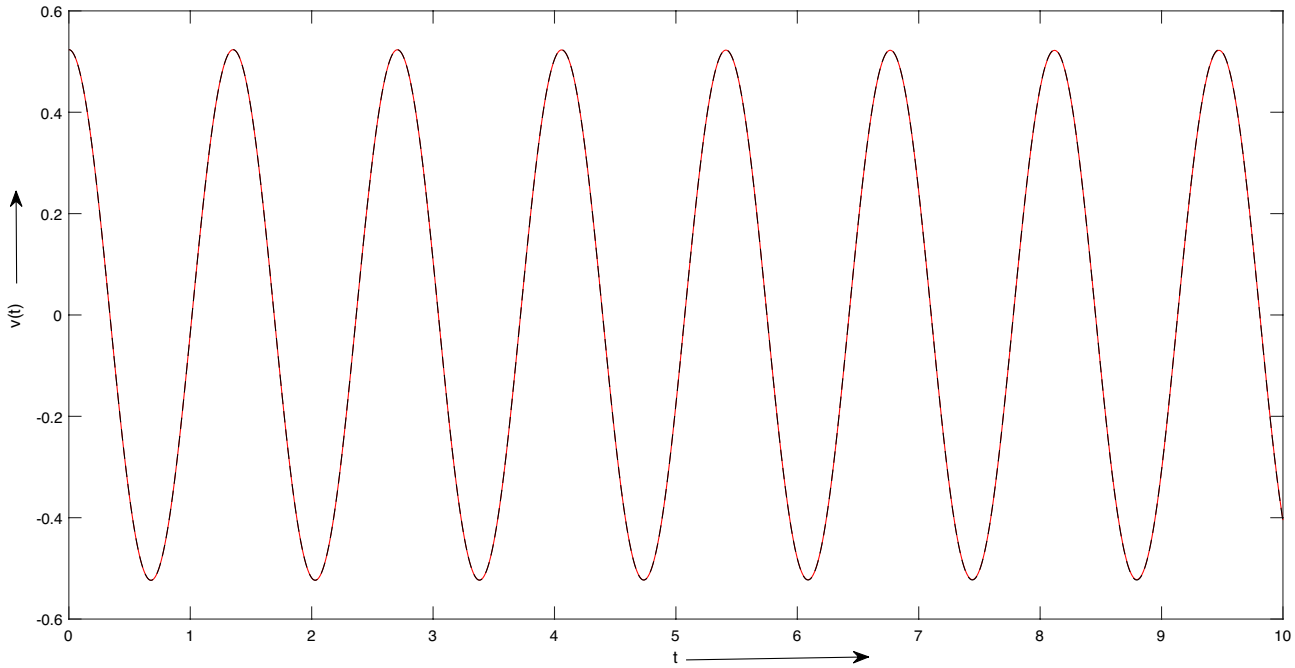

Figure 3. Case 1: Graph representation of solutions Example 4.1.

The problem represented by Eqs. (18) and (19) was numerically solved using the bvp5c function in MATLAB, as detailed in references[55]. The analysis revealed that the computed maximum error was approximately 9.779×10^{-11}.

A comprehensive examination of the results in Table 1 unequivocally demonstrates the superior performance of the LSHPM over AGM[16]. The LSHPM consistently delivers uniform results throughout the entire domain. In stark contrast, the HPM and AGM methods exhibit diminishing convergence as one moves away from the initial point, as illustrated by the data at $x = 2.7$ and $x = 3$ in Table 1.

The numerical solution of the problem represented by Eqs. (18) and (19) was carried out using MATLAB's bvp5c function, as detailed in references[55]. The computed maximum error was found to be on the order of 9.779×10^{-11}.

Analysis of the results presented in Table 1 clearly indicates the superior performance of the LSHPM over the AGM[16]. LSHPM consistently delivers uniform results throughout the entire domain, in stark contrast to the HPM and AGM, which exhibits diminishing convergence as one moves away from the initial point, as illustrated by the data at $x = 2.7$ and $x = 3$ in Table 1.

Example 4.2 By taking $A = 0.25$, $\Lambda = \frac{\pi}{3}$, we rewrite the problem (17) as

$$\frac{\mathrm{d}^2}{\mathrm{d}t^2}\theta + \frac{3}{4}\theta - \frac{1}{40}\theta^5 = 0, \tag{31}$$

$$\theta(0) = A, \quad \frac{d\theta}{dt}|_{t=0} = 0. \tag{32}$$

Initially, we formulate a homotopy for Eq. (31) as follows

$$H(\theta, p) = (1-p)\left(\frac{\mathrm{d}^2}{\mathrm{d}t^2}\theta + \frac{3}{4}\theta\right) + p\left(\frac{\mathrm{d}^2}{\mathrm{d}t^2}\theta + \frac{3}{4}\theta - \frac{1}{40}\theta\right)^5 = 0. \tag{33}$$

After substituting $\theta = \theta_0 + p\theta_1 + p^2 v_2 + p^3\theta_3 + \cdots$ into Eq. (33) and performing some simplification and rearrangement based on the powers of p, we have the following system of differential equations

$$p^0 : \left\{ \frac{\mathrm{d}^2}{\mathrm{d}t^2}\theta_0 + \frac{3}{4}\theta_0 = 0, \right. \tag{34}$$

$$p^1 : \left\{ \frac{\mathrm{d}^2}{\mathrm{d}t^2}\theta_1 + \frac{3}{4}\theta_1 - \frac{1}{40}\theta_0^5 = 0, \right. \tag{35}$$

$$p^2 : \left\{ \frac{\mathrm{d}^2}{\mathrm{d}x^2}\theta_2 + 0.75\,\theta_2 - 0.1250000000\,\theta_1\theta_0^4 = 0, \right. \tag{36}$$

$$\vdots$$

By solving equations (34) through (36) and applying the appropriate initial conditions, we can determine the parameters θ_0, θ_1, and θ_2. It is essential to emphasize that, apart from Eq. (34), the remaining equations are solved assuming zero initial conditions. Combining the solutions from Eqs. (34)–(36), we can derive an approximate HPM solution for Eq. (31), expressed as follows:

$$\theta = \theta_0 + \theta_1 + \theta_2.$$

This implies

$$\begin{aligned} \theta = {} & 0.01152903607\, t \sin\left(\hat{\alpha}\, t\right) + 1.053490429 \cos\left(\hat{\alpha}\, t\right) - 0.00006162350038\, t^2 \cos\left(\hat{\alpha}\, t\right) - \\ & 0.0001423133782\, t \sin\left(\hat{\alpha}\, t\right) \cos^2(\alpha t) - 0.004519692720 \cos^3(\alpha t) - \\ & 0.00009487558549\, t \sin\left(\hat{\alpha}\, t\right) \cos^4(\alpha t) - 0.001802399444 \cos^5(\alpha t) + \\ & 0.00002483198831 \cos^7(\alpha t) + 0.000004382115584 \cos^9(\alpha t), \end{aligned} \tag{37}$$

where $\hat{\alpha} = 0.866025404$ and $\alpha = 4.686149806$. It follows that (37) consist of $t \sin\left(\hat{\alpha}\, t\right)$, $\cos\left(\hat{\alpha}\, t\right)$, $t^2 \cos\left(\hat{\alpha}\, t\right)$, $t \sin\left(\hat{\alpha}\, t\right) \cos^2(\alpha t), \cos^3(\alpha t)$, $t \sin\left(\hat{\alpha}\, t\right) \cos^4(\alpha t)$, $\cos^5(\alpha t)$, $\cos^7(\alpha t)$, $\cos^9(\alpha t)$.

With this information, we propose that our trial solution for Eq. (31) within the LSHPM framework takes the following form

$$\begin{aligned} \tilde{\theta} = {} & c_0 \cos^9(\alpha t) + c_1 \cos^7(\alpha t) + c_2 \cos^5(\alpha t) + c_3 t \sin\left(\hat{\alpha}\, t\right) \cos^4(\alpha t) \\ & + c_4 \cos^3(\alpha t) + c_5 t \sin\left(\hat{\alpha}\, t\right) \cos^2(\alpha t) + c_6 \cos\left(\hat{\alpha}\, t\right) + c_7 \cos^2(\alpha t) + c_8 \sin\left(\hat{\alpha}\, t\right) t. \end{aligned} \tag{38}$$

Replacing $\tilde{\theta}$ for θ in Eq. (32), and applying the boundary conditions described in (32) through (38), we derive the following results

$$c_0 = \frac{\pi}{3} - c_1 - c_2 - c_4 - c_6. \tag{39}$$

Substituting (39) in (38), we have

$$\begin{aligned}\tilde{\theta} = (\frac{\pi}{3} - c_1 - c_2 - c_4 - c_6)\cos^9(\alpha t) + c_1\cos^7(\alpha t) + c_2\cos^5(\alpha t) + c_3 t\sin\left(\hat{\alpha}, t\right)\cos^4(\alpha t)\\ + c_4\cos^3(\alpha t) + c_5 t\sin\left(\hat{\alpha}\, t\right)\cos^2(\alpha t) + c_6\cos\left(\hat{\alpha}\, t\right) + c_7\cos\left(\hat{\alpha}\, t\right)t^2 + c_8\sin\left(\hat{\alpha}\, t\right)t.\end{aligned}$$

Replacing $\tilde{\theta}$ for θ in Eq. (31),We establish the residual function as

$$\hat{R}(t, c_1, c_2, c_3, c_4, c_5, c_6, c_7, c_8) = \frac{\mathrm{d}^2}{\mathrm{d}t^2}\tilde{\theta}(t) + 3/4\,\tilde{\theta}(t) - 1/40\left(\tilde{\theta}(t)\right)^5. \tag{40}$$

The error associated with the squared residual function is calculated as

$$J(c_1, c_2, c_3, c_4, c_5, c_6, c_7, c_8) = \int_0^3 \hat{R}^2(t, c_1, c_2, c_3, c_4, c_5, c_6, c_7, c_8)\, dt. \tag{41}$$

The optimal values for the variables represented as c_i (with i ranging from 1 to 8) can be determined by calculating the partial derivatives $\frac{\partial J}{\partial c_i}$ (provided in equation 41) using the software MAPLE 2016. Once these optimal values are identified, they can be substituted into the proposed solution as outlined in Eq. (38). Thus, we obtain:

$$\begin{aligned}\tilde{\theta}(t) = {} & 0.000002040196957\left(\cos\left(\hat{\alpha}\, t\right)\right)^9 + 0.00002558107881\left(\cos\left(\hat{\alpha}\, t\right)\right)^7 -\\ & 0.001795429257\left(\cos\left(\hat{\alpha}\, t\right)\right)^5 - 0.00009499027043\,\sin\left(\hat{\alpha}\, t\right)\left(\cos\left(\hat{\alpha}\, t\right)\right)^4 t -\\ & 0.004520492279\left(\cos\left(\hat{\alpha}\, t\right)\right)^3 - 0.0001411065420\,\sin\left(\hat{\alpha}\, t\right)\left(\cos\left(\hat{\alpha}\, t\right)\right)^2 t +\\ & \left(1.053485851 - 0.00006121848538\, t^2\right)\cos\left(\hat{\alpha}\, t\right) + 0.01153294833\,\sin\left(\hat{\alpha}\, t\right)t,\end{aligned} \tag{42}$$

where $\hat{\alpha} = 0.866025404$. The graphical representations of the HPM solution (37) and the LSHPM solution (41) are illustrated in Fig. 4, and the numerical results for both the above mentioned HPM solution are presented in the Table 2 below

Discussion of results of Example 4.2

The numerical solution for the problem described by Eqs. (31) and (32) was carried out using MATLAB's bvp5c functionality, with reference to[56]. The calculated maximum error was determined to be approximately 2.203×10^{-14}. A comprehensive assessment of the outcomes outlined in Table 2 unmistakably demonstrates the superior performance of the LSHPM over AGM[16] and the Homotopy Perturbation Method (HPM). LSHPM consistently yields uniform results across the entire domain, in stark contrast to AGM and HPM, which display diminishing convergence as one moves away from the initial point, as evident in the data from $x = 1.2$ to $x = 3$ in Table 2.

Analysis of results

It is worth noting that we utilized software, specifically MAPLE 2016, to solve Example 4.1 and Example 4.2. The computational time for these examples was remarkably efficient, taking only 10 seconds for the former and 3166 seconds for the latter. In Eqs. (29) and (41), we employed Riemann sums with 250 partitions to approximate the integrals.

t	bvp5c	AGM[16]	HPM	LSHPM	$\lvert AGM - bvp5c\rvert$	$\lvert HPM - bvp5c\rvert$	$\lvert LSHPM - bvp5c\rvert$
0	1.047197551196598	1.0471975	1.047197550939894	1.047197551196598	5.12×10^{-8}	0	0
0.3	1.013424671727360	1.013424	1.013424669235789	1.013424683416030	6.71×10^{-7}	2.23×10^{-9}	1.17×10^{-8}
0.6	0.913974676081452	0.91393499	0.913974568049639	0.913974673027138	3.97×10^{-5}	1.08×10^{-7}	3.08×10^{-9}
0.9	0.754613093042295	0.75422333	0.754612307207641	0.754613068460900	3.89×10^{-4}	7.86×10^{-7}	2.47×10^{-8}
1.2	0.545187482426038	0.54340399	0.545185016157168	0.545187481834252	1.78×10^{-3}	2.47×10^{-6}	6.15×10^{-10}
1.5	0.299304758127733	0.29405221	0.299299962043787	0.299304750241314	5.25×10^{-3}	4.79×10^{-6}	7.94×10^{-9}
1.8	0.033344937498370	0.02180802	0.033337895380757	0.033344898483015	1.15×10^{-2}	7.04×10^{-6}	3.91×10^{-8}
2.1	− 0.234852897025061	− 0.25534761	− 0.234861718041070	− 0.234852915665731	2.05×10^{-2}	8.82×10^{-6}	1.87×10^{-8}
2.4	− 0.487292693627270	− 0.51818573	− 0.487302480151352	− 0.487292697296632	3.09×10^{-2}	9.79×10^{-6}	3.72×10^{-9}
2.7	− 0.707109264825293	− 0.74765086	− 0.707118292264257	− 0.707109310645214	4.05×10^{-2}	9.03×10^{-6}	4.59×10^{-8}
3.0	− 0.879899013158141	− 0.92648305	− 0.879904794111942	− 0.879899025013068	4.66×10^{-2}	5.78×10^{-6}	1.19×10^{-8}

Table 2. Comparison of HPM, LSHPM, AGM and bvp5c results when $A = 0.25$, $\Lambda = \frac{\pi}{3}$.

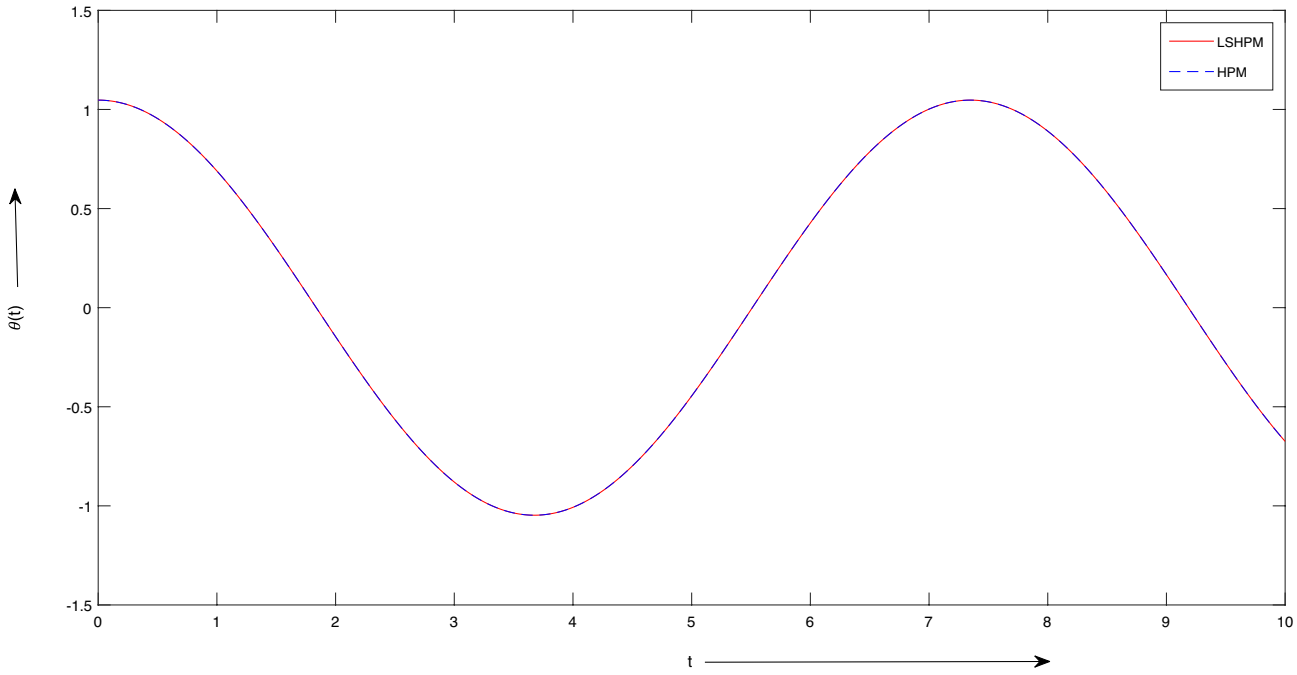

Figure 4. Graph of solutions of Example 4.2.

Validation

We have validated the three methods, HPM, LSHPM, and the numerical method using MATLAB's builtin function bvp5c for both Examples as illustrated in Table 1 and Table 2. As shown in these tables, it is clear that HPM and LSHPM work better and are more accurate than AGM[16] in this investigation. In "Analysis of results" section, we provide a detailed description of the initial conditions for both scenarios. As this study primarily aims to assess the influence of individual parameters on the system's response, we employ LSHPM with a variety of initial conditions to examine the results. Next, we delve into the analysis of Case 1.

The results presented for case 1:

- For Fig. 5, we take $K = 100 Newton/meter^2$, $g = 9.8\ meter/sec^2$, $m_1 = 5\ Kg$ $m_2 = 1\ Kg$, $L = 1\ meter$, $A = [\frac{\pi}{24}, \frac{\pi}{12}, \frac{\pi}{8}, \frac{\pi}{6}, \frac{\pi}{3}]meter$. Figure 5 reveal that changes in amplitude have no discernible impact on the

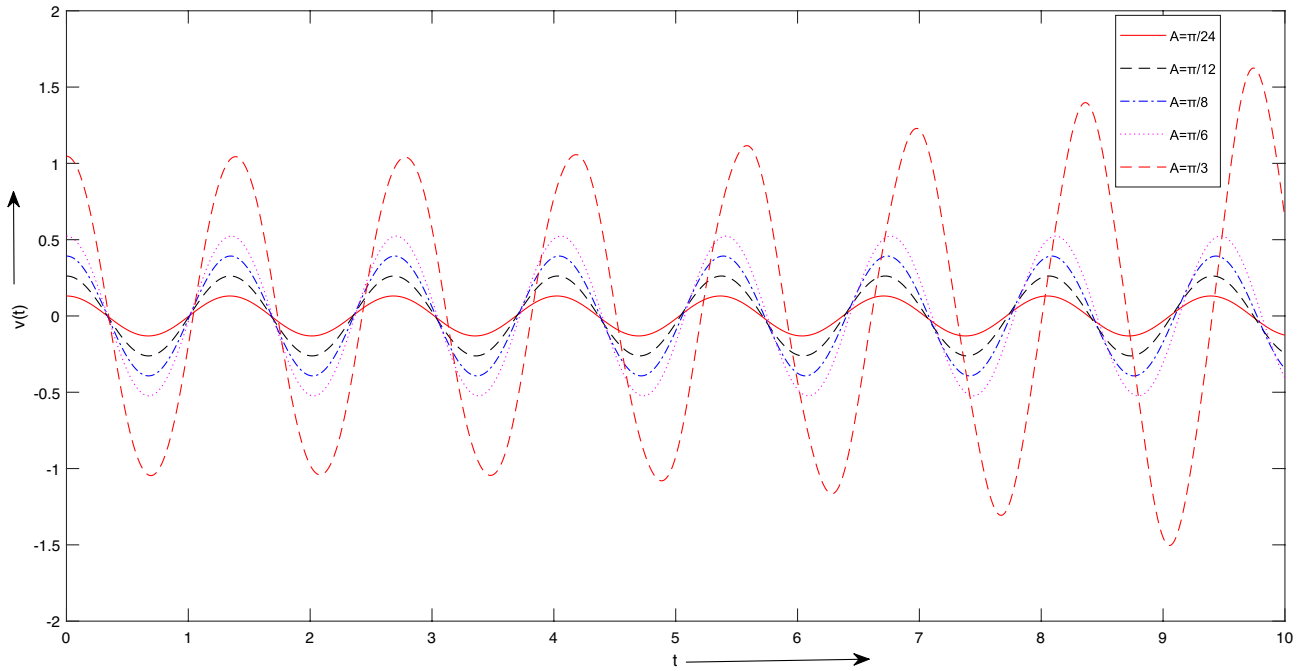

Figure 5. Case 1. Graph for LSHPM solutions with different inititial conditions *A*.

period or frequency; nonetheless, they exert a significant influence on the system's behavior. In oscillatory systems, the count and regularity of oscillations are fundamental attributes. It is feasible to scrutinize the motion of the system and ascertain the quantity of oscillations occurring within a defined time frame through the resolution of the equations of motion.

- For Fig. 6, we take the values as: $K = [50, 100, 300] Newton/meter^2, g = 9.8\ meter/sec^2, m_1 = 5\ Kg\, m_2 = 1\ Kg$, $L = 1\ meter, A = \frac{\pi}{6}, \frac{\pi}{3}]meter$. Figure 6 depicts that as the stiffness increases, there is a noticeable decrease in the duration of the oscillation's period. Specifically, when the stiffness value is elevated from 50 to 300,

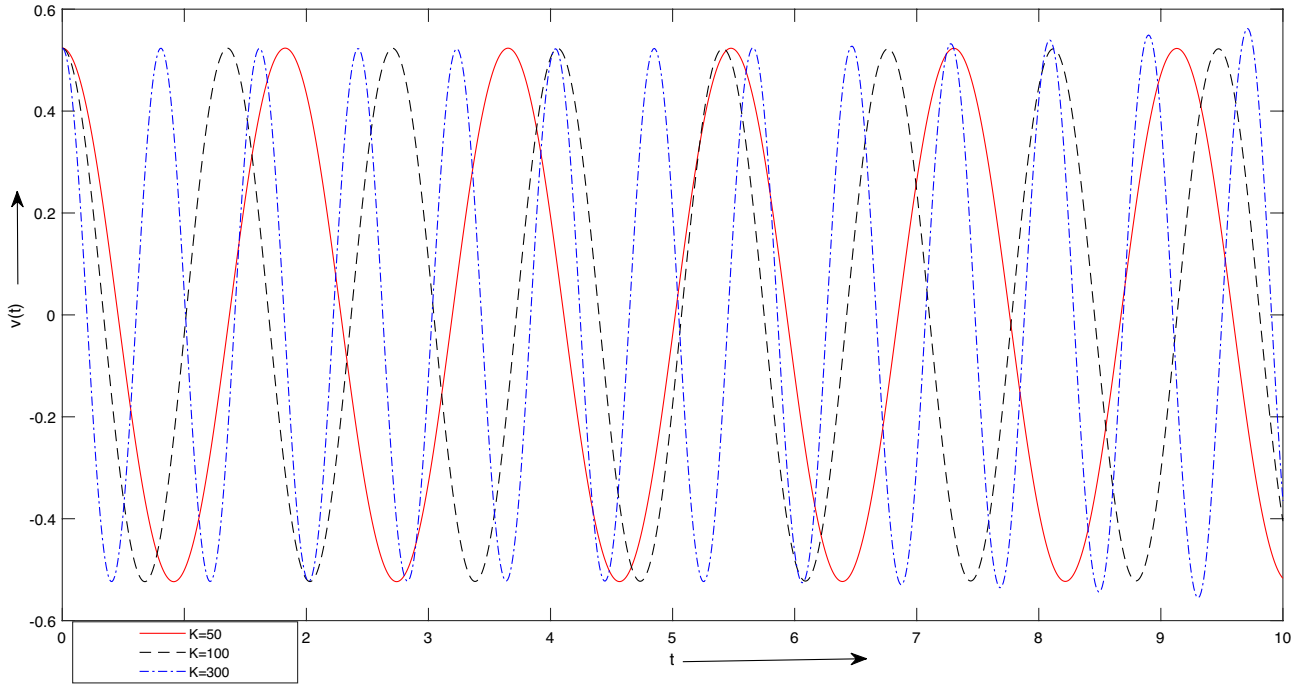

Figure 6. Case 1. Graph for LSHPM solutions with different values of K.

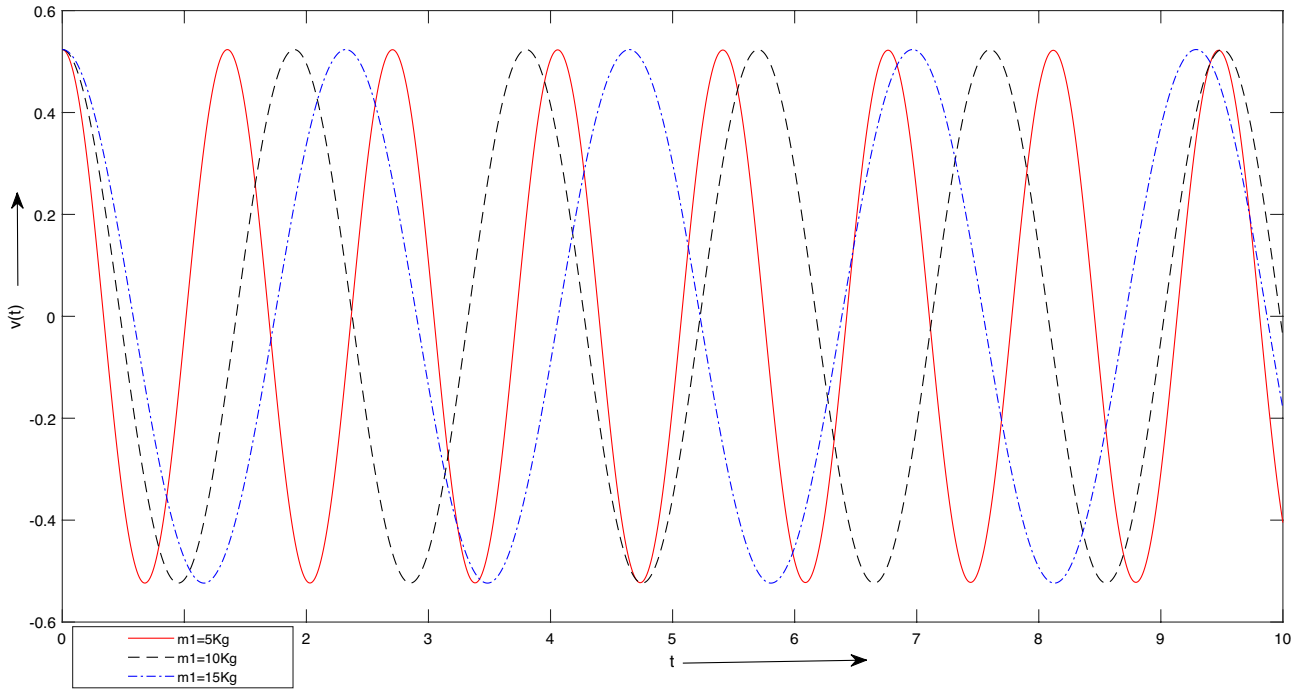

Figure 7. Case 1. Graph for LSHPM solutions with different values of m_1.

the period time diminishes from approximately two seconds to less than one second within a three-second interval.

- For Fig. 7, we take $K = 100 Newton/meter^2$, $g = 9.8\ meter/sec^2$, $m_1 = [5,\ 10,\ 15]\ Kg$, $m_2 = 1\ Kg$, $L = 1\ meter, A = \frac{\pi}{6}, \frac{\pi}{3}]meter$. The findings in Fig. 7 suggest that an increase in mass results in an extended period of oscillation. This occurs because as the mass of the block increases, the system's inertia also increases, leading to a reduction in frequency. This behavior closely resembles the observations in Fig. 6, where stiffness modifications produced analogous effects.
- For Fig. 7, we take $K = 100 Newton/meter^2, g = 9.8\ meter/sec^2, m_1 = 5\ Kg, m_2 = 1\ Kg, L = [1,\ 2,\ 3]\ meter$, $A = \frac{\pi}{6}, \frac{\pi}{3}]meter$. Figure 8 provides insights into the influence of increasing the length parameter, denoted as L, on the period of oscillation. It is observed that augmenting the length results in a minor extension of the oscillation period. However, this particular parameter exerts a less pronounced effect on the system's temporal response and frequency when compared to other variables. Additionally, Fig. 8 illustrates the consequences of altering amplitudes on the system's temporal behavior. Any adjustments in amplitude manifest as changes in the slope of the curves, signifying an increase in angular velocity. Notably, these alterations in amplitude do not significantly impact the system's oscillation period.

The results presented for case 2:

- For Fig. 9, we take $\Lambda = \frac{\pi}{3}$, A =[0.5, 1, 1.5]. Figure 9 depicts how various amplitudes impact the time response of the system. It is evident that alterations in amplitude result in a more or less abrupt shift in the slope of the lines, signifying an increase in angular velocity. As shown in Fig. 9, adjustments in amplitude do not significantly influence the system's period time.
- For Fig. 10, we consider $A = \frac{\pi}{3}$, Λ =[0.5, 1, 1.5]. Figure 10 demonstrates the impact of varying Λ values on the system's time response. Once again, a noticeable shift in time response is observed when significant changes occur in the parameter Λ, as depicted in Fig. 10.

In upcoming endeavors, our approach will involve the utilization of LSHPM alongside the MATLAB built-in function bvp5c for the resolution of diverse mathematical models that encompass nonlinear ordinary, partial, and fractional differential equations.

Conclusion

In our investigation, we utilized three different approaches-MATLAB's built-in function bvp5c, HPM, and LSHPM-to explore two distinct oscillating systems, comparing their results against numerical solutions. The comparative error analysis for both cases, as presented in Tables 1 and 2, highlights the effectiveness of these methods in dealing with oscillating systems. Notably, LSHPM demonstrated superior convergence rates and higher accuracy when compared to AGM and HPM, as clearly indicated in Tables 1 and 2.

The adaptability of these methods was demonstrated by modifying individual parameters, such as stiffness or length, showcasing LSHPM's ability to deliver highly accurate results closely aligned with numerical values.

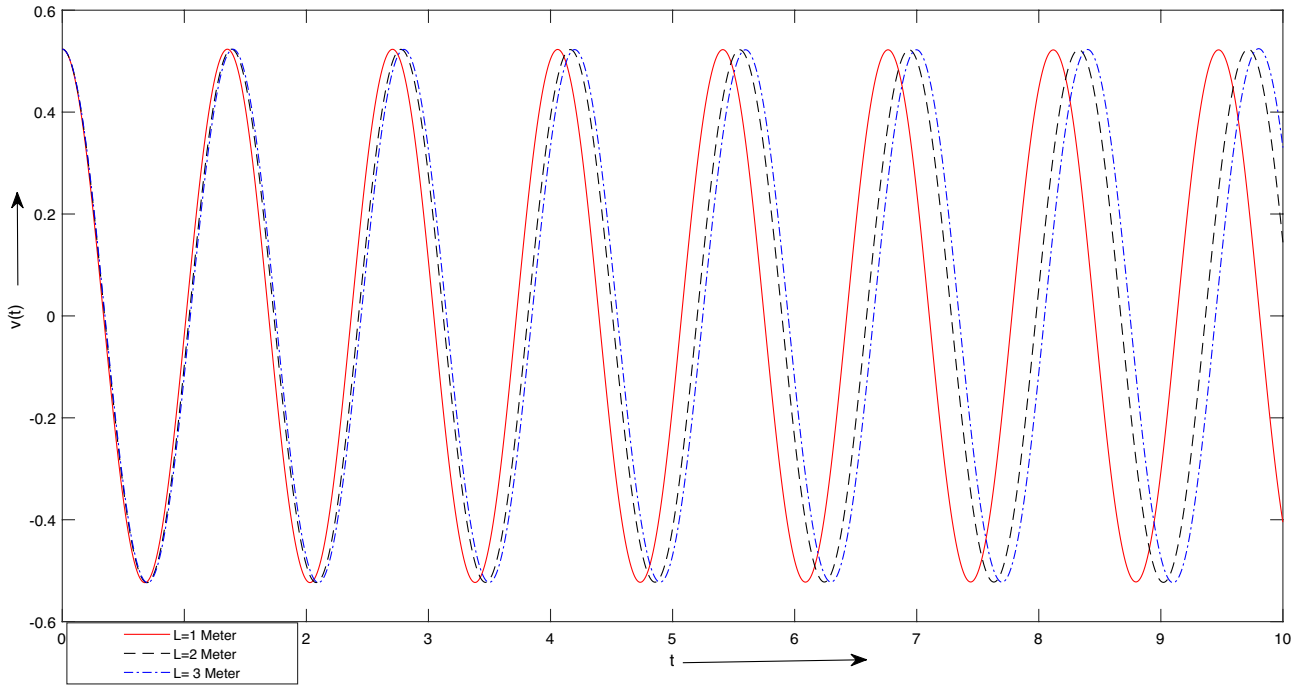

Figure 8. Case 1. Graph for LSHPM solutions with different values of *l*.

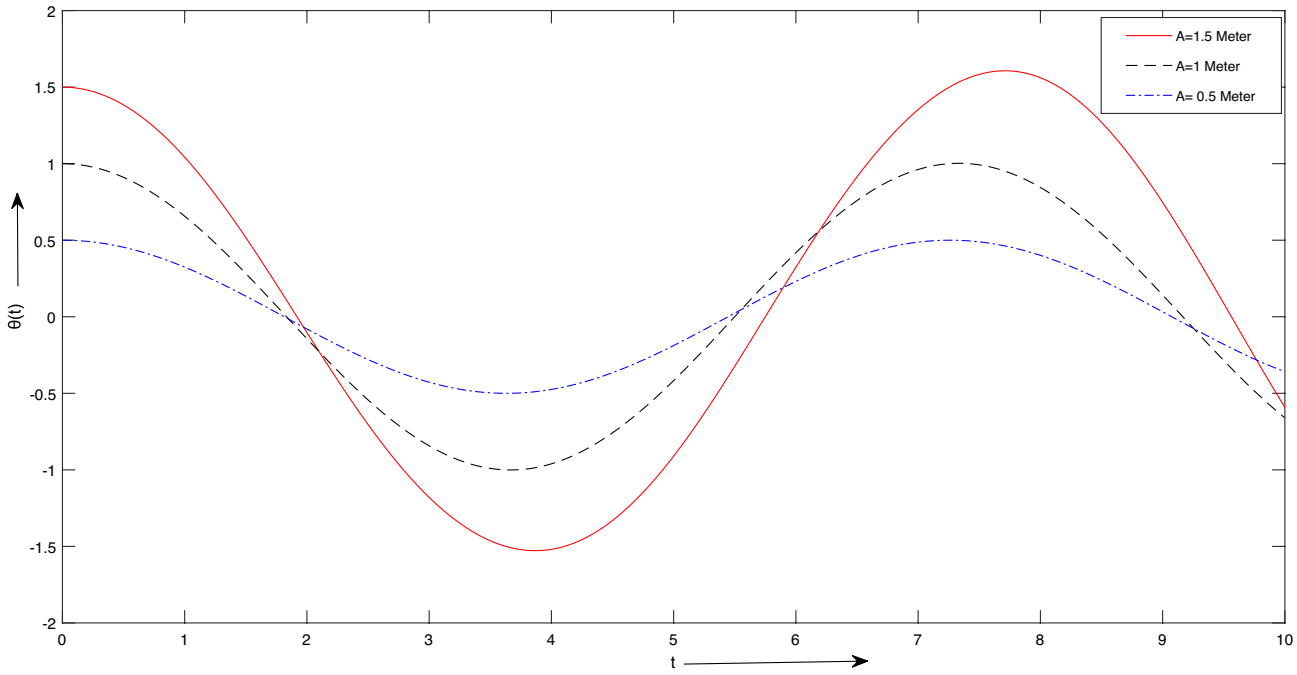

Figure 9. Case 2. Graph for different initial conditions A.

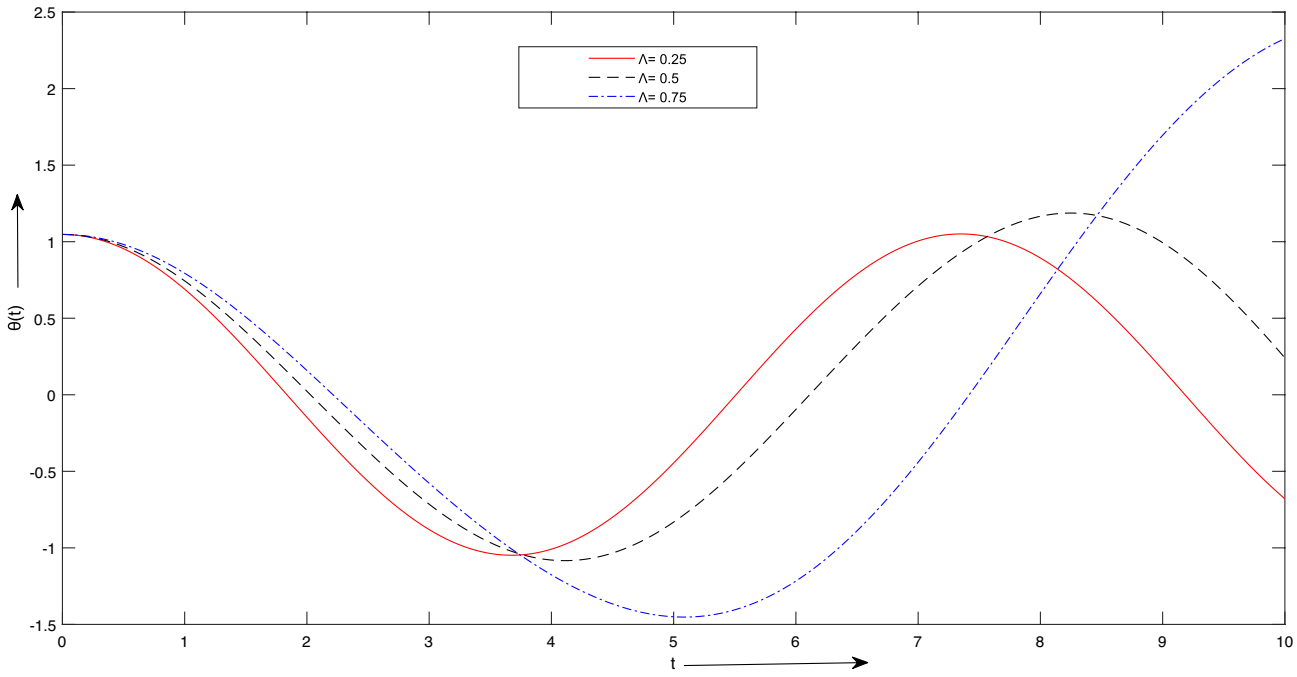

Figure 10. Case 2. Graph of solutions for different values of Λ.

Furthermore, the exploration of various parameters revealed that stiffness significantly influenced the system's period time, while mass and length had inverse effects. Importantly, variations in length were observed to have a relatively milder impact on the system's temporal response and frequency when compared to changes in stiffness and mass.

Data availibility

All data generated or analyzed during this study are included in this published article.

Received: 9 November 2023; Accepted: 8 January 2024
Published online: 17 January 2024

References

1. Lazutkin, G., Davydov, D., Varzhitskiy, L., Boyarov, K. & Volkova, T. Non-linear oscillations of mechanical systems with structure damping vibration protection devices. *Procedia Eng.* **176**, 334–343 (2017).
2. Ibsen, L., Barari, A. & Kimiaeifar, A. Analysis of highly nonlinear oscillation systems using he's max–min method and comparison ith homotopy analysis and energy balance methods. *Sadhana* **35**, 433–448. https://doi.org/10.1007/s12046-010-0024-y (2010).
3. Decuyper, J., De Troyer, T., Runacres, M., Tiels, K. & Schoukens, J. Nonlinear state-space modelling of the kinematics of an oscillating circular cylinder in a fluid flow. *Mech. Syst. Signal Process.* **98**, 209–230 (2018).
4. Yang, K., Joshua Yang, J., Huang, R. & Yang, Y. Nonlinearity in memristors for neuromorphic dynamic systems. *Small Sci.* **2**, 2100049 (2022).
5. Kumar, S., Chauhan, R., Momani, S. & Hadid, S. Numerical investigations on Covid-19 model through singular and non-singular fractional operators. *Numer. Methods Part. Differ. Equ.* **6**, 66 (2020).
6. Kumar, S., Kumar, A., Samet, B. & Dutta, H. A study on fractional host-parasitoid population dynamical model to describe insect species. *Numer. Methods Part. Differ. Equ.* **37**, 1673–1692 (2021).
7. Mohammadi, H., Kumar, S., Rezapour, S. & Etemad, S. A theoretical study of the Caputo–Fabrizio fractional modeling for hearing loss due to mumps virus with optimal control. *Chaos Solitons Fract.* **144**, 110668 (2021).
8. Qian, H. & Bishop, L. M. The chemical master equation approach to nonequilibrium steady-state of open biochemical systems: Linear single-molecule enzyme kinetics and nonlinear biochemical reaction networks. *Int. J. Mol. Sci.* **11**, 3472–3500 (2010).
9. Eusebi Borzelli, G. L. & Carniel, S. A reconciling vision of the Adriatic–Ionian bimodal oscillating system. *Sci. Rep.* **13**, 2334 (2023).
10. Aydiner, E. Anomalous cyclic in the neutrino oscillations. *Sci. Rep.* **13**, 12651 (2023).
11. Hałgas, S. A spice-oriented method for finding multiple dc solutions in nonlinear circuits. *Appl. Sci.* **13**, 2369 (2023).
12. Sun, N., Wu, Y., Fang, Y. & Chen, H. Nonlinear antiswing control for crane systems with double-pendulum swing effects and uncertain parameters: Design and experiments. *IEEE Trans. Autom. Sci. Eng.* **15**, 1413–1422 (2017).
13. Seth, G. S., Bhattacharyya, A., Kumar, R. & Mishra, M. K. Modeling and numerical simulation of hydromagnetic natural convection Casson fluid flow with nth-order chemical reaction and Newtonian heating in porous medium. *J. Porous Media* **22**, 66 (2019).
14. Kundu, S., Muruganandam, P., Ghosh, D. & Lakshmanan, M. Amplitude-mediated spiral chimera pattern in a nonlinear reaction–diffusion system. *Phys. Rev. E* **103**, 062209 (2021).
15. Henriques, J., Portillo, J., Sheng, W., Gato, L. & Falcão, A. d. O. Dynamics and control of air turbines in oscillating-water-column wave energy converters: Analyses and case study. *Renew. Sustain. Energy Rev.* **112**, 571–589 (2019).
16. Samadi, H., Shams Mohammadi, N., Shamoushaki, M., Asadi, Z. & Domiri Ganji, D. An analytical investigation and comparison of oscillating systems with nonlinear behavior using agm and hpm. *Alex. Eng. J.***61**, 8987–8996. https://doi.org/10.1016/j.aej.2022.02.036 (2022).
17. Ushijima, S., Nezu, I. & Okuyama, Y. Numerical prediction for transportation of non-uniform particles accumulated under oscillating turbulent flows. In Matsuno, K., Ecer, A., Satofuka, N., Periaux, J. & Fox, P. (Eds.) *Parallel Computational Fluid Dynamics 2002* 531–538 (North-Holland, 2003). https://doi.org/10.1016/B978-044450680-1/50067-X.
18. Xie, G., Lei, J., Deng, X., Wang, J. & Chen, H. Numerical investigation on two-phase oscillating flow and heat transfer enhancement for a cooling channel with ribs. *Int. J. Therm. Sci.* **187**, 108191. https://doi.org/10.1016/j.ijthermalsci.2023.108191 (2023).
19. Sfahani, M., Barari, A., Omidvar, M., Ganji, S. & Domairry, G. Dynamic response of inextensible beams by improved energy balance method. *Proc. Inst. Mech. Eng. Part K J. Multi-body Dyn.* **225**, 66–73 (2011).
20. Ganji, S., Ganji, D. & Karimpour, S. He's energy balance and he's variational methods for nonlinear oscillations in engineering. *Int. J. Mod. Phys. B* **23**, 461–471 (2009).
21. Afzal, S., Qayyum, M. & Chambashi, G. Heat and mass transfer with entropy optimization in hybrid nanofluid using heat source and velocity slip: A Hamilton–Crosser approach. *Sci. Rep.* **13**, 12392 (2023).
22. Ganji, D. D. & Azimi, M. Application of max min approach and amplitude frequency formulation to nonlinear oscillation systems. *UPB Sci. Bull.* **74**, 131–140 (2012).
23. Qie, N., Houa, W.-F. & He, J.-H. The fastest insight into the large amplitude vibration of a string. *Rep. Mech. Eng.* **2**, 1–5 (2021).
24. Mohammadian, M. & Shariati, M. Application of ag method and its improvement to nonlinear damped oscillators. *Sci. Iran.* **27**, 203–214 (2020).
25. El-Dib, Y. O. Homotopy perturbation method with rank upgrading technique for the superior nonlinear oscillation. *Math. Comput. Simul.* **182**, 555–565 (2021).
26. Ullah, H. *et al.* Mhd boundary layer flow over a stretching sheet: A new stochastic method. *Math. Probl. Eng.* **2021**, 1–26 (2021).
27. Khan, I. *et al.* Falkner–Skan equation with heat transfer: A new stochastic numerical approach. *Math. Probl. Eng.* **2021**, 1–17 (2021).
28. Khan, R. A. *et al.* Heat transfer between two porous parallel plates of steady nano fludis with Brownian and thermophoretic effects: A new stochastic numerical approach. *Int. Commun. Heat Mass Transf.* **126**, 105436 (2021).
29. Khan, M. A., Ullah, S. & Kumar, S. A robust study on 2019-ncov outbreaks through non-singular derivative. *Eur. Phys. J. Plus* **136**, 1–20 (2021).
30. Kumar, S., Kumar, R., Cattani, C. & Samet, B. Chaotic behaviour of fractional predator–prey dynamical system. *Chaos Solitons Fract.* **135**, 109811 (2020).
31. Kumar, S., Kumar, R., Osman, M. & Samet, B. A wavelet based numerical scheme for fractional order seir epidemic of measles by using genocchi polynomials. *Numer. Methods Part. Differ. Equ.* **37**, 1250–1268 (2021).
32. Ullah, H. *et al.* Neuro-computing for hall current and mhd effects on the flow of micro-polar nano-fluid between two parallel rotating plates. *Arab. J. Sci. Eng.* **47**, 16371–16391 (2022).
33. Ullah, H. *et al.* Intelligent computing of Levenberg–Marquard technique backpropagation neural networks for numerical treatment of squeezing nanofluid flow between two circular plates. *Math. Probl. Eng.* **6**, 66 (2022).
34. Bilal, H. *et al.* A Levenberg–Marquardt backpropagation method for unsteady squeezing flow of heat and mass transfer behaviour between parallel plates. *Adv. Mech. Eng.* **13**, 16878140211040896 (2021).
35. Shoaib, M. *et al.* Heat transfer impacts on Maxwell nanofluid flow over a vertical moving surface with mhd using stochastic numerical technique via artificial neural networks. *Coatings* **11**, 1483 (2021).
36. Jawad, M., Shah, Z., Khan, A., Islam, S. & Ullah, H. Three-dimensional magnetohydrodynamic nanofluid thin-film flow with heat and mass transfer over an inclined porous rotating disk. *Adv. Mech. Eng.* **11**, 1687814019869757 (2019).
37. Khan, A. *et al.* Darcy–Forchheimer flow of mhd cnts nanofluid radiative thermal behaviour and convective non uniform heat source/sink in the rotating frame with microstructure and inertial characteristics. *AIP Adv.* **8**, 66 (2018).
38. Fiza, M., Ullah, H. & Islam, S. Three-dimensional mhd rotating flow of viscoelastic nanofluid in porous medium between parallel plates. *J. Porous Media* **23**, 66 (2020).
39. Ullah, H., Islam, S. & Fiza, M. Analytical solution for three-dimensional problem of condensation film on inclined rotating disk by extended optimal homotopy asymptotic method. *Iran. J. Sci. Technol. Trans. Mech. Eng.* **40**, 265–273 (2016).
40. Ullah, H., Islam, S., Khan, I., Bin Shafie, S. & Fiza, M. Mhd boundary layer flow of an incompressible upper convected Maxwell fluid by optimal homotopy asymptotic method. *Sci. Iran.* **24**, 202–210 (2017).
41. Fiza, M., Islam, S., Ullah, H. & Ali, Z. Mhd thin film oldroyd-b fluid with heat and viscous dissipation over oscillating vertical belts. *Heat Transf. Res.* **50**, 66 (2019).

42. Fiza, M., Ullah, H., Islam, S., Nasir, S. & Khan, I. Analytical solution of heat transfer and unsteady flow of second-grade fluid past a porous, moving, and oscillating vertical belt. *Heat Transf. Res.* **50**, 66 (2019).
43. Akbar, A. *et al.* Intelligent computing paradigm for the Buongiorno model of nanofluid flow with partial slip and mhd effects over a rotating disk. *ZAMM-J. Appl. Math. Mech./Zeitschrift für Angewandte Mathematik und Mechanik* **103**, e202200141 (2023).
44. Akbar, A. *et al.* A design of neural networks to study mhd and heat transfer in two phase model of nano-fluid flow in the presence of thermal radiation. *Waves Random Complex Media* **66**, 1–24 (2022).
45. Ullah, H. *et al.* Numerical treatment of squeezed mhd jeffrey fluid flow with Cattaneo Chrisstov heat flux in a rotating frame using Levnberg–Marquard method. *Alex. Eng. J.* **66**, 1031–1050 (2023).
46. Ullah, H. *et al.* Levenberg–Marquardt backpropagation for numerical treatment of micropolar flow in a porous channel with mass injection. *Complexity* **2021**, 1–12 (2021).
47. Khan, I. *et al.* Fractional analysis of mhd boundary layer flow over a stretching sheet in porous medium: A new stochastic method. *J. Funct. Spaces* **2021**, 19 (2021).
48. Sayevand, K. & Jafari, H. On systems of nonlinear equations: Some modified iteration formulas by the homotopy perturbation method with accelerated fourth-and fifth-order convergence. *Appl. Math. Model.* **40**, 1467–1476 (2016).
49. Shafiei, N., Kazemi, M., Safi, M. & Ghadiri, M. Nonlinear vibration of axially functionally graded non-uniform nanobeams. *Int. J. Eng. Sci.* **106**, 77–94 (2016).
50. Nourazar, S. & Nazari-Golshan, A. A new modification to homotopy perturbation method combined with Fourier transform for solving nonlinear Cauchy reaction diffusion equation. *Indian J. Phys.* **89**, 61–71 (2015).
51. Qayyum, M. & Oscar, I. Least square homotopy perturbation method for ordinary differential equations. *J. Math.* **2021**, 1–16 (2021).
52. Qayyum, M. *et al.* Fractional analysis of unsteady squeezing flow of Casson fluid via homotopy perturbation method. *Sci. Rep.* **12**, 18406 (2022).
53. Fathollahi, R., Alizadeh, A., Kamaribidkorpeh, P., Abed, M. A. & Pasha, P. Analyzing the effect of radiation on the unsteady 2d mhd al2o3-water flow through parallel squeezing sheets by agm and hpm. *Alex. Eng. J.* **69**, 207–219. https://doi.org/10.1016/j.aej.2022.11.035 (2023).
54. Kierzenka, J. & Shampine, L. F. A bvp solver that controls residual and error. *J. Numer. Anal. Ind. Appl. Math.* **3**, 27–41 (2008).
55. Vedavathi, N., Dharmaiah, G., Noeiaghdam, S. & Fernandez-Gamiz, U. A chemical engineering application on hyperbolic tangent flow examination about sphere with Brownian motion and thermo phoresis effects using bvp5c. *Case Stud. Therm. Eng.* **40**, 102491. https://doi.org/10.1016/j.csite.2022.102491 (2022).
56. Anwar Beg, O., Zohra, F., Uddin, M., Ismail, A. & Sathasivam, S. Energy conservation of nanofluids from a biomagnetic needle in the presence of Stefan Blowing: Lie symmetry and numerical simulation. *Case Stud. Therm. Eng.* **24**, 100861. https://doi.org/10.1016/j.csite.2021.100861 (2021).

Acknowledgements

The authors are thankful to the Heads of their institutions for providing excellent research environment.

Author contributions

Conceptualization: M.R.; Formal analysis: H.A.; Investigation: A.S.; Methodology: M.R.; Software: M.R.; Re-Graphical representation and Adding analysis of data: H.A. and A.S.; Writing—original draft: M.R.; Writing—review editing: H.A. and A.S.; Re-modelling design: A.S.; Re-Validation: A.S.; M.K.; Prepared Rebuttal, Proof-read. Furthermore, all the authors equally contributed to the writing and proofreading of the paper. All authors reviewed the manuscript.

Competing interests

The authors declare no competing interests.

Additional information

Correspondence and requests for materials should be addressed to A.S.

Reprints and permissions information is available at www.nature.com/reprints.

Publisher's note Springer Nature remains neutral with regard to jurisdictional claims in published maps and institutional affiliations.